Heliyon 10 (2024) e34682

Contents lists available at ScienceDirect

Heliyon

journal homepage: www.cell.com/heliyon

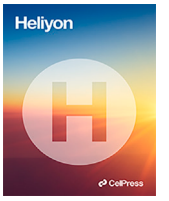

Research article

Symmetric optical multipass matrix systems and the general rapid design methodology

Xiangjun Xiao [1], Miyun Shi [1], Jingjing Qiu, Xue Ou, Peng Liu, Xin Zhou *

Center for Advanced Quantum Studies, Applied Optics Beijing Area Major Laboratory, Department of Physics, Beijing Normal University, Beijing 100875, China

ARTICLE INFO

Keywords:
Multipass matrix systems
Evolutionary optimization algorithm
Optical path length

ABSTRACT

We proposed an original type of multipass cell named symmetric optical multipass matrix system (SMMS), in which the same matrix patterns of various sizes can be formed on both sides. According to its special symmetric configurations, the SMMS design problem is modeled as a variant of the classical traveling salesman problem, which can be rapidly solved by evolutionary optimization algorithms. Two sets of 3-mirror SMMSs are designed, analyzed and built, which show superior characteristics of high stability, desirable beam quality and adjustable optical path lengths. Additionally, they can support simultaneous detection of multiple species with multi-laser channels. The proposed method is further extended to design a 4-mirror SMMS, which verifies the universality and robustness of the design methodology. The experimental observations are in consistent with the theoretical calculations. The newly proposed SMMSs have a broad application prospect in trace gas measurement.

1. Introduction

Laser spectroscopic trace-gas sensing technology is important for monitoring and increasing the understanding of greenhouse gas and air pollutant emissions, atmospheric chemistry and industrial processes [1,2]. Tunable diode laser absorption spectroscopy (TDLAS) has become an important and powerful tool for the detection of trace gases in industry and research due to its high sensitivity, good accuracy and selectivity [3–6]. Multipass cells (MPCs) with long optical path lengths (OPLs) are key components in the TDLAS technique. MPC design can be a significant contributor to achieving drastic improvement in TDLAS detection sensitivity. An ideal MPC for trace gas sensing should have the following attributes:
(1) A long effective optical path length (typically path lengths up to several hundred meters are needed) [7].
(2) Desired spot pattern with perfect regularity and easy identification of reflections and optical path length [8].
(3) High utilization rate of the mirror surfaces [9].
(4) Good optomechanical stability. In particular, the MPC should be insensitive to thermal changes and mechanical vibrations [10].
(5) Simplicity of alignment and pathlength adjustment [11].
(6) Support for multiple beam pathlength (for simultaneous multiple species detection) [12,13].
(7) Cost-effective (e.g. the use of standard concave spherical mirrors).

* Corresponding author.
E-mail address: zhoux@bnu.edu.cn (X. Zhou).
[1] These authors contributed equally to this work.

https://doi.org/10.1016/j.heliyon.2024.e34682
Received 5 December 2023; Received in revised form 15 July 2024; Accepted 15 July 2024

Available online 18 July 2024

Recently, various types of MPCs have been employed for gas detection successfully, such as Herriott-type cells [14], White-type cells [15] and toroidal type cells [16,17]. A classical Herriott cell consists of two identical spherical mirrors facing each other. The effective utilization rate of the mirror surfaces is comparatively small. To overcome such drawbacks, some researchers use a pair of astigmatic mirrors instead of spherical mirrors to form complex Lissajous spot patterns [18,19]. However, the cost of making highly precise astigmatic mirrors is prohibitively high. Some researchers, in recent years, have designed Herriott-type cells with concentric and independent circular patterns, which have obvious regularity and a high optical path length to volume ratio [9,10,20–23]. Nevertheless, spot deformation is serious and too complex to analyze meticulously. Additionally, the distance between the two spherical mirrors is relatively small that the optical path length is usually in the range of a few meters or tens of meters. Hence such MPCs are more suitable for making miniaturized portable devices.

A White cell [15], including its improvements, possesses three spherical mirrors of equal curvature radius. A mirror is placed at a distance equal to the radius of curvature from the other two mirrors. This kind of cell can form one or two rows of spots, but the aberration is serious, and the stability is poor. A matrix spot pattern can be formed by adding optical elements such as sets of mirrors, cubic angles or prisms to the White cell [11]. Such a design significantly increases the optical path length and improves the stability of the system. However, the introduction of the non-spherical elements may cause significant errors to the pass of the light [24]. In 1991, Chernin proposed two versions of optical multipass matrix systems (MMSs). One set is composed of a primary mirror and an auxiliary field mirror placed relative to three objective mirrors, and the other set is equipped with four objective mirrors [25–28]. By changing the placement angle of the mirrors, matrix patterns of even rows and arbitrary columns can be formed on the primary mirror of the MMSs but not on the other side. In 2016, Guo designed an optical system composed of four asymmetric spherical mirrors to enhance the robustness of the Chernin's four-objective MMS [29]. Two years later, he made further improvements to this by using slicer mirrors to reduce alignment difficulty and improve system compactness [30].

In 2013, T. Mohamed designed a cell with a confocal placement of three mirrors to three mirrors, which achieved relatively uniform spot patterns on both sides of the cell [31]. In 2021, Xia searched parameters randomly in a cell with the same structure, forming matrix patterns on both sides. The incomplete matrix patterns on the two sides were not symmetric [7], and the search time for the design parameters of the cell was as long as two days.

MMSs effectively overcome the severe aberration and poor stability of the traditional White cell. They have high utilization ratio of mirrors and very long adjustable optical pathlengths, which are suitable for trace gas monitoring. Table 1 shows the comparison of different confocal MPCs (especially MMSs) with spherical mirrors. The previous designs are not ideal and lack of general rapid design strategies. The newly designed SMMSs overcome the deficiencies that the inlet and outlet windows are adjacent, and can form adjustable matrix on both sides. Under the special symmetric configurations, only one side of the system should be considered during the design process, which greatly reduces the dimension of the complex problem. Based on the confocal principle, the design process of the matrix patterns on one side can be modeled as a variant of the classical traveling salesman problem, which can be rapidly solved by intelligent optimization algorithms. As a result, two sets of 3-mirror SMMSs are designed, analyzed and built, which show superior characteristics of high stability, desirable beam quality and adjustable optical path from a few meters to several hundred meters. Additionally, they can support simultaneous detection of multiple species with multi-laser channels. The proposed method is further extended to design a 4-mirror SMMS, which verify the universality and robustness of the design methodology. The experimental observations are in good agreement with the theoretical calculations. The newly proposed SMMSs have a broad application prospect in trace gas measurement.

2. The principles of designing SMMSs and a traveling salesman problem model

On account of the special symmetric configurations, only mirrors and image patterns on one side of the system should be considered during the design process. Based on the confocal principle, object and image points lie on a straight line that has its midpoint at the curvature center of the reflecting mirror [15], the design process of the matrix patterns on one side can be modeled as a matrix traveling salesman problem (matrix-TSP). Therefore, the complex three-dimensional problem of beam propagation in a confocal MPC with multiple spherical mirrors can be simplified to a two-dimensional problem with discrete variables.

A matrix pattern with m rows and n columns contains mn images. The initial image with an access order of 0 is fixed in the upper-right corner of the matrix, and the remaining images are recorded as $v = \{v_1, v_2, ..., v_{mn-1}\}$. The variable to be solved is the access order of all the remaining images $p = (p_1, p_2, ..., p_{mn-1})$, with $p_i \in v(i = 1, 2, ..., mn - 1)$. The constraint is that each image should be visited only once. The number of midpoints of all successive access images N represents the number of curvature centers of the opposite side mirrors. The optimization goal for matrix-TSP is to $\min\{|N\text{-}3|\}$, and the optimal solution is the formation order of the matrix pattern on one side of the system. The matrix-TSP can be easily solved in various methods. Many kinds of evolutionary optimization algorithms are very efficient in solving such problems. We took a genetic algorithm (GA) with order encoding coded in MATLAB, which can easily find the best solutions of the problem with appropriate scales in several minutes. The solution of the matrix-TSP is the formation order of the matrix pattern on one side of an SMMS. To realize symmetric matrix patterns and mirror configurations on two sides, we invert the image formation order to obtain the formation sequence of the matrix pattern on the other side. Considering the image formation order on two sides, the images can be classified into different specular surfaces. We will try to extend the row and column of the matrix if it can be divided into three nonoverlapping rectangular parts.

The 3-mirror SMMS design strategy proposed in this paper can be adapted to design 4-mirror SMMSs. The constraint condition is changed: each image can be accessed no more than twice. In addition, the optimization goal needs to be changed to $\min\{|N - 4|\}$ and the matrix pattern found is used on the inlet side. If the matrix pattern can be spatially divided into four nonoverlapping rectangular mirrors, a 4-mirror SMMS is successfully designed.

Table 1
Comparison of different confocal MPCs with spherical mirrors.

Type	Ref.	Rows×Columns[a]	Mirror Number	Matrix on:	Adjacent In/Out	Adjustable OPL	Overlap
Previous research							
White	[15]	$1\times n$	1,2	field	No	Yes	No
	[32]	$2\times n$	1,2	field	No	Yes	No
	[33]	$m\times 2$	1,2	field	Yes	Yes	No
Shetter et al.	[34]	$m\times n$[b]	1,m	field	No	Yes	No
Chernin (3-mirror)	[25]	$m(even)\times n$	2,3	field	Yes	Yes	No
	[27]	$m(even)\times n$	2,3	field	No	Yes	No
Chernin (4-mirror)	[25]	$m(even)\times n$	2,4	field	Yes	Yes	Yes
	[28–30]	$m(odd)\times n$	2,4	field	No	Yes	Yes
T. Mohamed	[31]	disorderly pattern	3,3	both	Yes[c]	No	Yes
Jin Baoxia	[7]	Incomplete matrix	3,3	both	Yes[c]	No	Yes
Present design							
3-mirror SMMS-I		$m(even)\times n$	3,3	both	No[d]	Yes	No
3-mirror SMMS-II		$m(even)\times n$	3,3	both	No[d]	Yes	No
4-mirror SMMS		$m(even)\times n$[e]	4,4	both	No[d]	No[f]	Yes

[a] m, n are natural numbers, limited by the dimensions of the mirror.
[b] A matrix with some distortion.
[c] The beam exits through the same hole from which it entered the system.
[d] The inlet/outlet beam is separated to two sides of the system, which provides great convenience for system assembly.
[e] There are some missing matrices.
[f] OPL is not easy to adjust in an established system but available to choose in a wide range for practical use.

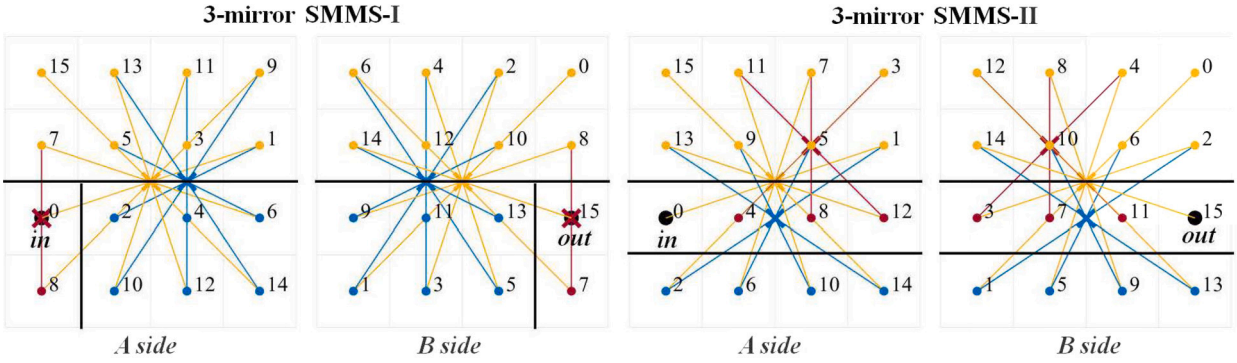

Fig. 1. Two kinds of 3-mirror SMMS configurations and matrix patterns. The inlet window is 'in', and the outlet window is 'out'. Points of different colors represent images on different mirror surfaces. The curvature centers of mirrors on one side are represented on the opposite side by crosses with the same color. The object and image points corresponding to the curvature centers are connected by the same color. The numbers to the right of the points indicate the order of matrix formation. Black lines separate the mirrors.

3. Results

3.1. Construction of 3-mirror SMMSs

After searching for an hour, we finally designed two sets of 3-mirror SMMSs, 3-mirror SMMS-I and 3-mirror SMMS-II. The configuration of both sides of the systems and the formation orders of the matrix patterns of 3-mirror SMMSs are shown in Fig. 1. The B side shows the matrix pattern which is the solution of the matrix-TSP, representing the formation sequence of images at the outlet side of SMMS-I and II; the A side shows the formation sequence of images at the inlet side of SMMS-I and II, with an opposite order to that of the B side.

3-mirror SMMS-I and 3-mirror SMMS-II both have two sets of three concave spherical rectangular mirrors of the same size, and all mirrors have the same radius of curvature R, which equals the distance between the A side and the B side of the system. A Cartesian coordinate system is defined with the origin at the midpoint of the line that connects the geometric center of mirrors at two sides, and the direction of the z-axis is along this line. The row and column spacing of the matrix are represented by d_l and d_c, respectively. $C_1 \sim C_6$ are the curvature centers of mirrors $M_1 \sim M_6$.

3.1.1. 3-mirror SMMS-I

The construction of SMMS-I is illustrated in Fig. 2(a). In 3-mirror SMMS-I, the length of $M_1\&M_4$, $M_2\&M_5$, $M_3\&M_6$ is nd_c, d_c, $(n-1)d_c$ along the x-axis, and $md_l/2$ along the y-axis. The positions of the inlet window, the first image on the B side, the outlet window, the curvature centers $C_1 \sim C_6$ are expressed as Eq. (1).

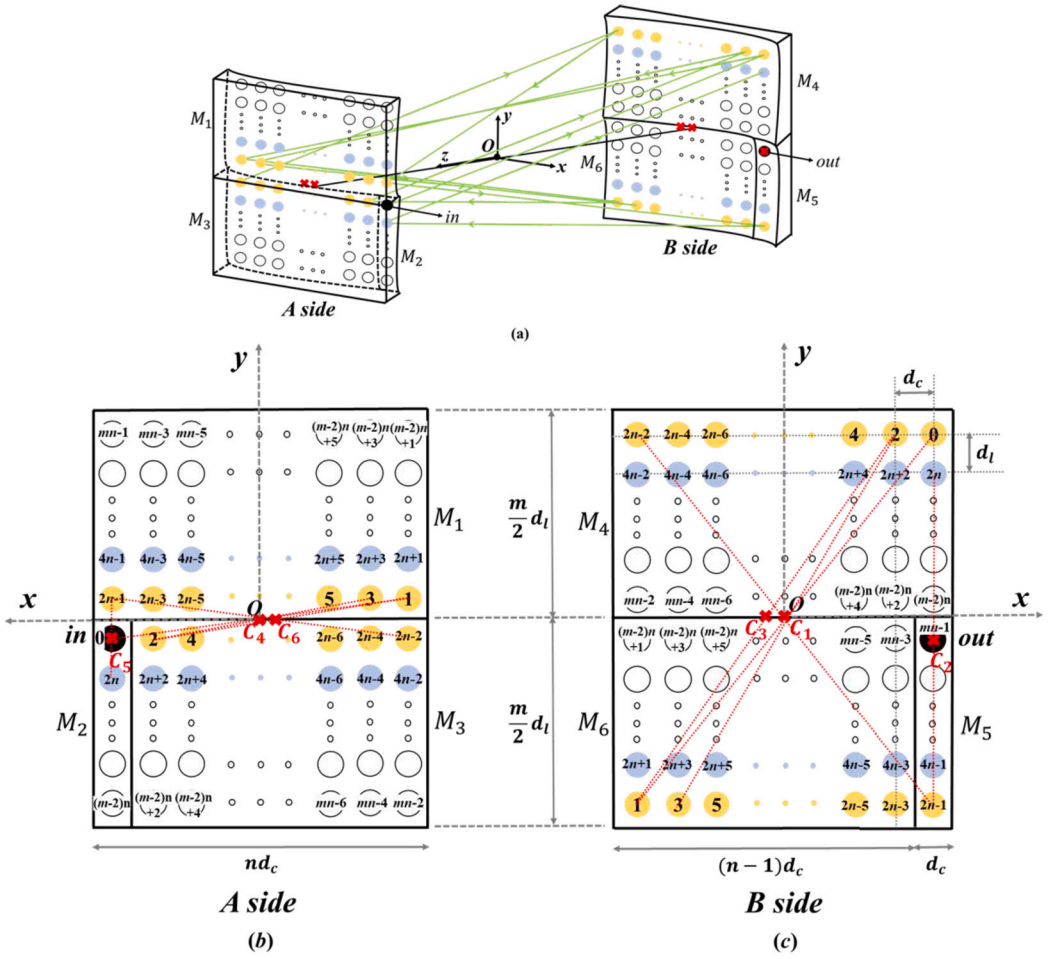

Fig. 2. The structure of 3-mirror SMMS-I. (a) 3D schematic diagram. (b) (c) 2D matrix patterns on both sides of the system.

$$
\begin{aligned}
&in(\frac{n-1}{2}d_c, -\frac{d_l}{2}, \frac{R}{2}) \quad B0(\frac{n-1}{2}d_c, \frac{m-1}{2}d_l, -\frac{R}{2})\\
&out(\frac{n-1}{2}d_c, -\frac{d_l}{2}, -\frac{R}{2})\\
&C_1(0,0,-\frac{R}{2}) \qquad C_2(\frac{n-1}{2}d_c, -\frac{1}{2}d_l, -\frac{R}{2})\\
&C_3(-\frac{1}{2}d_c, 0, -\frac{R}{2}) \qquad C_4(0,0,\frac{R}{2})\\
&C_5(\frac{n-1}{2}d_c, -\frac{1}{2}d_l, \frac{R}{2}) \quad C_6(-\frac{1}{2}d_c, 0, \frac{R}{2})
\end{aligned} \tag{1}
$$

As seen from the formation sequence of the image marked in Fig. 2 (b) and (c), the propagation mode of the optical rays in the system is as follows: light enters the system through the inlet window on the A side and creates image 0 on the B side. Conjugated mirrors M_1 and M_3 successively focus the inlet window image on the B side with a displacement of d_c to form two lines of images (denoted by yellow circles) until image $2n-1$ is formed on mirror M_5. Then, the light is reflected onto the A side, forming image $2n$, which has an offset shift by d_l relative to the entry position along the y-axis. As if it has been emitted from a new inlet window, the light is then directed to the B side, forming image $2n$ on mirror M_4, whose position is offset from image 0. To make image $2n$ and image 0 at the same place along the x-axis, the distance between curvature centers C_2 and C_1 must be equal to $(n-1)d_c/2$ along the x-axis. The distance between image $2n$ and 0, d_l, is twice as far away from curvature centers C_2 and C_1 along the y-axis. The shift of image $2n$ will cause the formation of the next pair of spots (denoted by blue circles) until image $4n-1$ forms on mirror M_5. The next pair of images will be shifted in turn on the basis of the above rules until the light passes through the outlet window. Then, a complete matrix pattern of m rows and n columns has been formed on the B side, and the same pattern has been formed on the A side by similar rules. If the light path is reversed in this system and the light is incident from the outlet window, the same result will be obtained as in the original system.

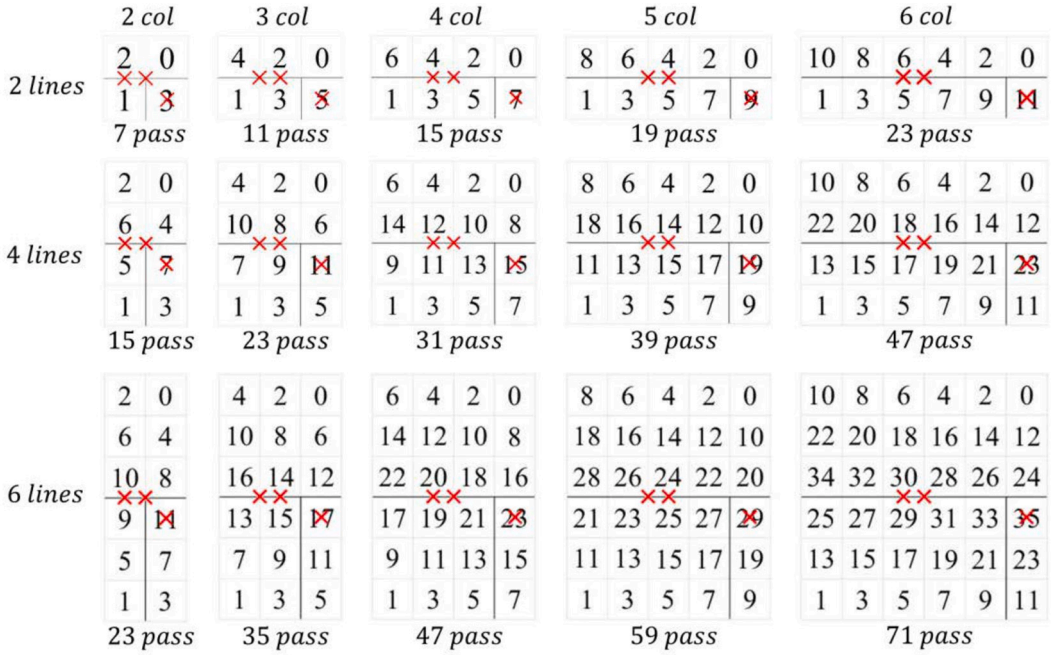

Fig. 3. Examples of matrix patterns (B side) of 3-mirror SMMS-I.

The number of the passages in SMMS-I is determined by the formula: $pass = 2m \cdot n - 1$, where the number of rows, m is an even number ($m = 2, 4, 6, \ldots$) and the number of columns, n is a natural number ($n = 2, 3, 4, \ldots$). When the inlet and outlet windows have relatively fixed positions to the mirrors, the number of rows and columns of matrix patterns can be changed by adjusting the incident direction and the positions of the curvature centers to obtain different optical path lengths required for measurement. When the row spacing is constant, if image 0 on the B side moves d_l along the positive or negative direction of the y-axis, the matrix increases or decreases by two rows. When the column spacing is constant, if the curvature centers C_1, C_3 and C_4, C_6 move $d_c/2$ in the positive or negative direction of the x-axis, the matrix decreases or increases by one column. Fig. 3 provides examples of matrix patterns on the B side. Each number represents an image and indicates its creation order. The red crosses are the curvature centers, and the black lines separate different mirrors.

3.1.2. 3-mirror SMMS-II

The construction of SMMS-II is illustrated in Fig. 4(a). In 3-mirror SMMS-II, the length of $M_1\&M_4$, $M_2\&M_5$, $M_3\&M_6$ is $md_l/2$, d_l, $(m/2-1)d_l$ along the y-axis, and nd_c along the x-axis. The positions of the inlet window, the first image on the B side, the outlet window, and the curvature centers $C_1 \sim C_6$ are expressed as Eq. (2).

$$
\begin{aligned}
&in(\frac{n-1}{2}d_c, -\frac{d_l}{2}, \frac{R}{2}) \quad B0(\frac{n-1}{2}d_c, \frac{m-1}{2}d_l, -\frac{R}{2}) \\
&out(\frac{n-1}{2}d_c, -\frac{d_l}{2}, -\frac{R}{2}) \\
&C_1(0, 0, -\frac{R}{2}) \quad C_2(-\frac{1}{2}d_c, \frac{m-2}{4}d_l, -\frac{R}{2}) \\
&C_3(0, -\frac{1}{2}d_l, -\frac{R}{2}) \quad C_4(0, 0, \frac{R}{2}) \\
&C_5(-\frac{1}{2}d_c, \frac{m-2}{4}d_l, \frac{R}{2}) \quad C_6(0, -\frac{1}{2}d_l, \frac{R}{2})
\end{aligned}
\tag{2}
$$

As seen from the formation sequence of the image marked in Fig. 4(b) and (c), the propagation mode of the optical rays in the system is as follows: Conjugated mirrors M_1 and M_3 successively focus the inlet window image on the B side with a displacement of d_l to form two columns of images (different pairs of columns are denoted by circles of different colors). When an image forms on mirror M_5, it will symmetrically offset with the center of C_2, thus forming a new pair of columns of images. After the beam passes through the outlet window, a complete matrix pattern of m rows and n columns is formed on the B side, and the same pattern is formed on the A side by similar rules.

The number of the passages in SMMS-II is determined by the formula: $pass = 2m \cdot n - 1$, where the number of rows, m is an even number ($m = 4, 6, \ldots$) and the number of columns, n is a natural number ($n = 1, 2, 3, \ldots$). When the inlet and outlet windows have relatively fixed positions to the mirrors, the number of rows and columns of the matrix patterns can be changed by adjusting the incident direction and the positions of the curvature centers to obtain different optical path lengths required for measurement. When

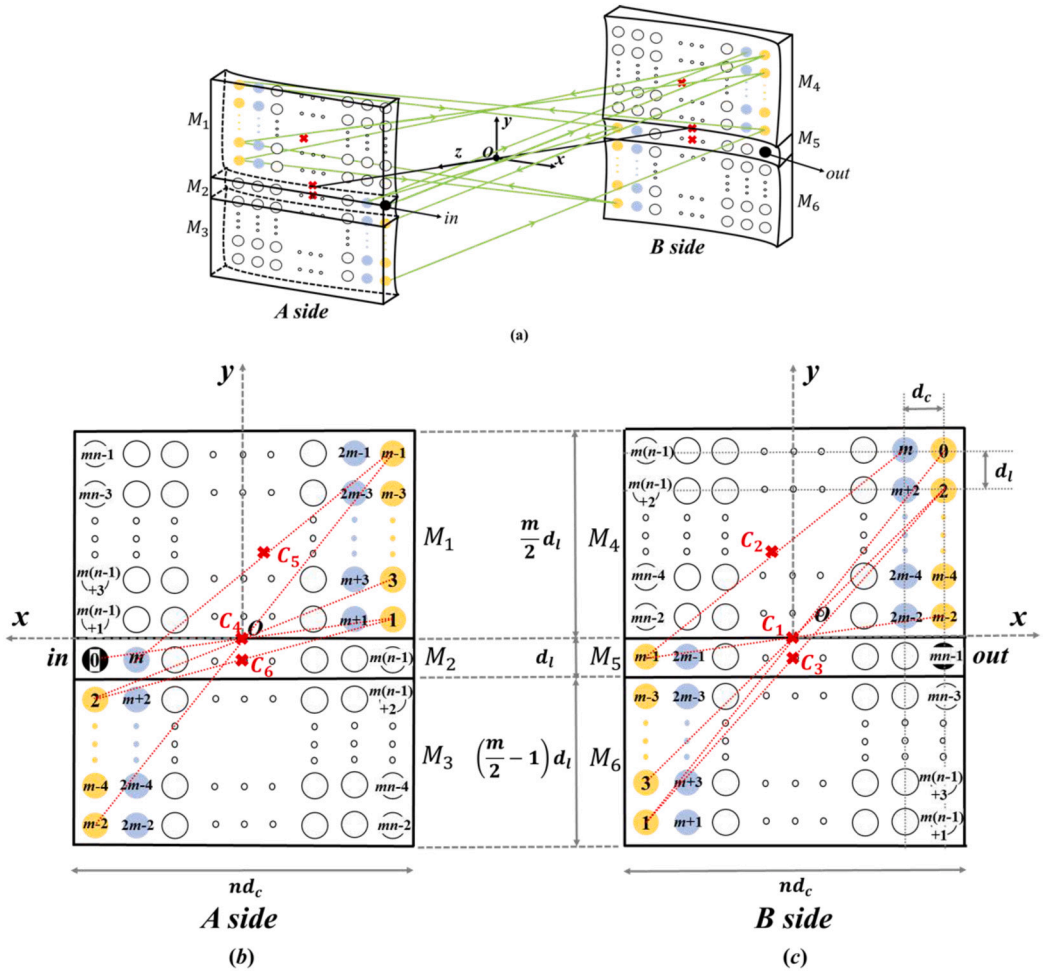

Fig. 4. The structure of 3-mirror SMMS-II. (a) 3D schematic diagram. (b) (c) 2D matrix patterns on both sides of the system.

the row spacing is constant, if image 0 on the B side moves d_l and curvature centers C_2 and C_5 move $d_l/2$ along the positive or negative direction of the y-axis, the matrix increases or decreases by two rows. When the column spacing is constant, if the curvature centers $C_1 \sim C_3$ and $C_4 \sim C_6$ move $d_c/2$ in the positive or negative direction of the x-axis, the matrix decreases or increases by one column. Fig. 5 provides examples of the matrix patterns on the B side. Each number represents an image and indicates its creation order. The red crosses are the curvature centers, and the black lines separate different mirrors.

3.2. Construction of 4-mirror SMMS

As shown in Fig. 6, we have found a matrix pattern that meets the requirements of the 4-mirror SMMS setup mentioned earlier. The inlet window is located at image 0 on the inlet side, while the outlet window is located at number 17 on the outlet side. When analyzing the pattern formation rule on the outlet side shown in Fig. 6, mirrors M_1&M_4 or M_2&M_3 on the outlet side and all the mirrors on the inlet side can be regarded as a set of White cell. The blue lines connect images formed by conjugate mirrors M_1 and M_4, while the green lines connect the images formed by M_2 and M_3. The matrix pattern on the outlet side can be formed in the same way.

We further expanded the matrix pattern to other rows and columns, taking Fig. 7(a) as a case in point. The first point is fixed on the curvature center of M_6 when expanding the matrix patterns. The matrices formed by this reflection law are missing in some rows and columns: some special matrices such as 8×5 and 8×11, the matrices with $n+(2n-1)x$ rows, n columns and the matrices with m rows, $m+(2m-1)x$ columns can not form completely, where $x=0,1,2,\ldots$. An incomplete matrix is formed under the following conditions: The object point happens to fall on the position of the curvature center that will form the next image point before forming a complete matrix. In this case, the object point, the image point and the related curvature center is located at an identical position. If there is no outlet window on the A side, the beam will leave the system from the inlet window in the direction opposite to the direction of incidence, which cause the complete matrix formation to be terminated. Fig. 7 (b) and (c) shows the examples of incomplete matrices of 8×5 and 4×4 respectively. Once the complete matrix is formed and the beam exit from the outlet window on the A side which is symmetrical to the inlet window on the B side, the number of the passages in a 4-mirror SMMS is: $pass=4mn-2(m+n)+1$.

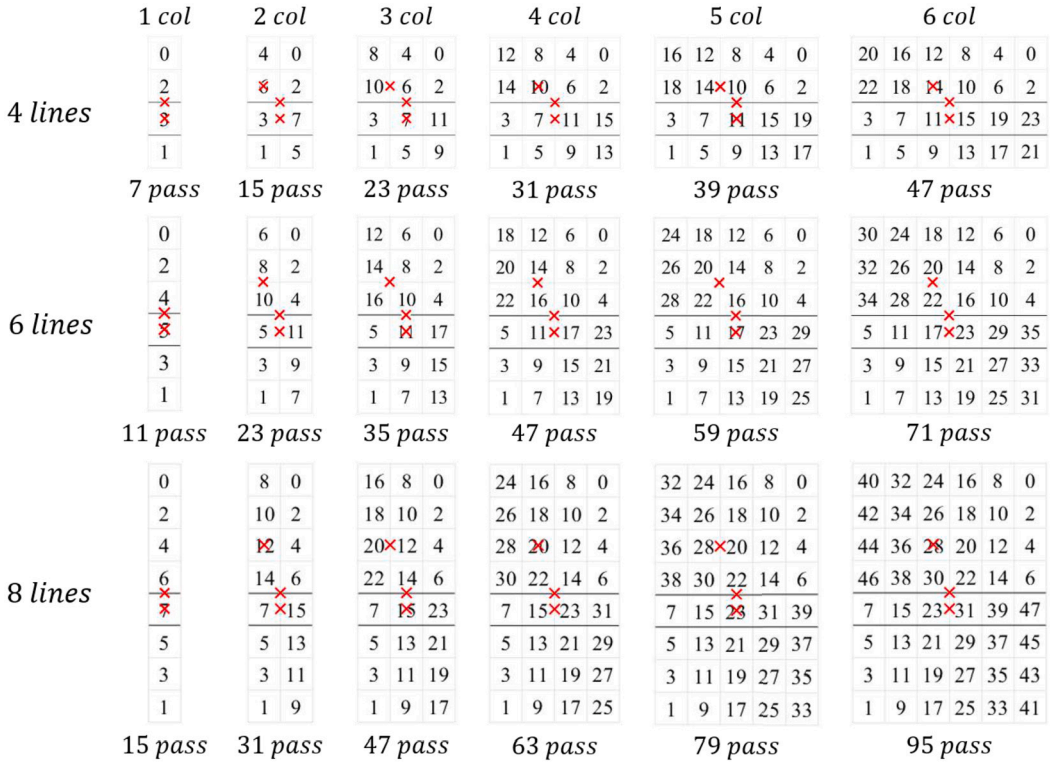

Fig. 5. Examples of matrix patterns (B side) of 3-mirror SMMS-II.

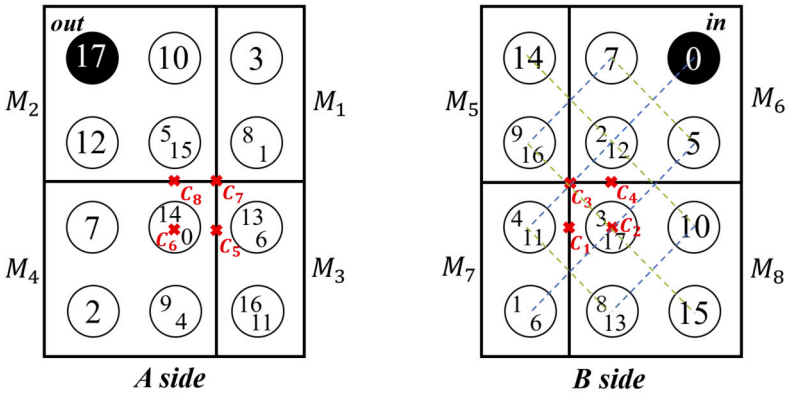

Fig. 6. The configuration and matrix pattern of the 4-mirror SMMS.

4. Discussion

4.1. Analysis of 3-mirror SMMSs

4.1.1. Stability analysis

Stability is an essential criterion in the design of an MPC. Due to mechanical vibrations in practical applications, there can be changes in the placement of mirrors and the angles of incidence. Hence it is important to analyze the stability of the configuration of 3-mirror SMMSs. When the positions of curvature centers $C_1 \sim C_3$ or image 0 on the A side are changed, the matrix pattern on the B side can be maintained as long as the corresponding images on the A side are still on their original mirrors. The rule also applies to changing the parameters of the B side. Owing to the symmetric construction of the systems, only the corresponding parameters located on one side must be analyzed. Therefore, slight disturbances are only introduced into the positions of image 0 and curvature center $C_1 \sim C_3$ located at the B side during the analysis. The following analysis holds true for both 3-mirror SMMS-I and II.

According to the principle of stability of even images in the MMS [35], it is better to mount the mirrors on the same side on a single plate or use one freedom surface instead of the original separated surfaces [36] to obtain greater stability. In this circumstance,

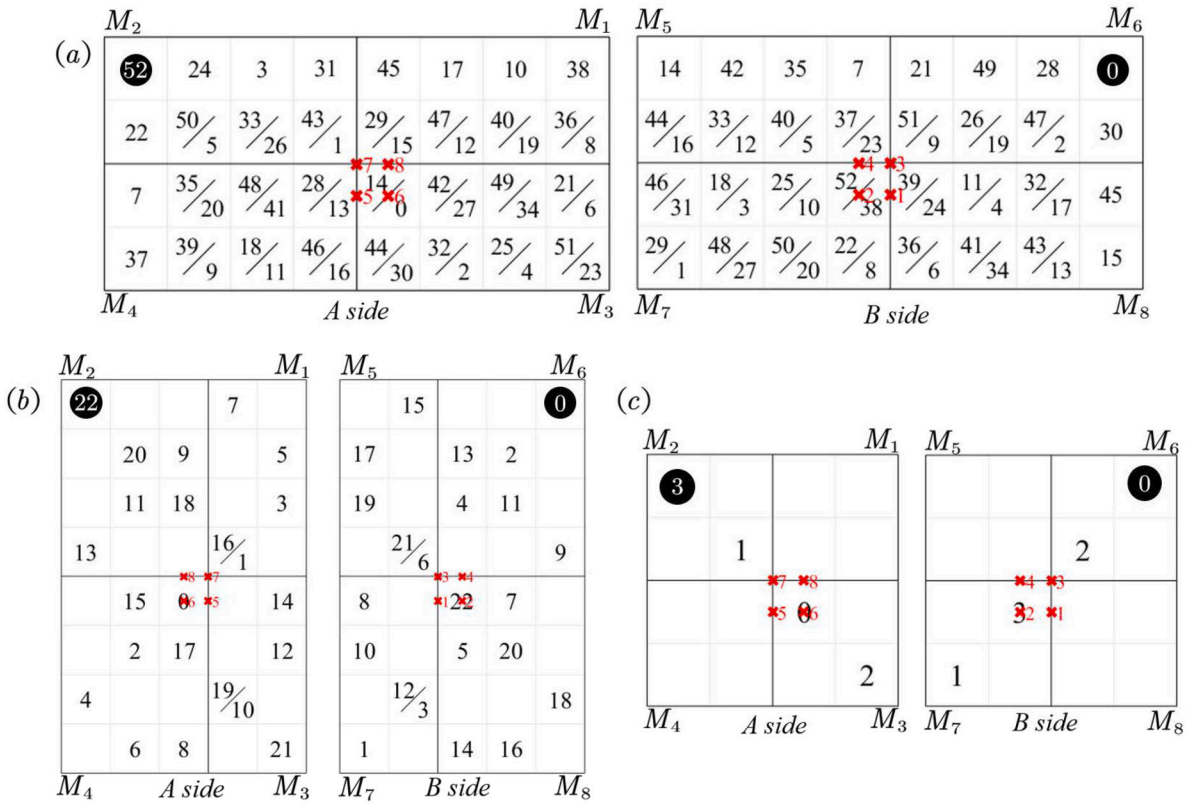

Fig. 7. Examples of patterns of 4-mirror SMMS.

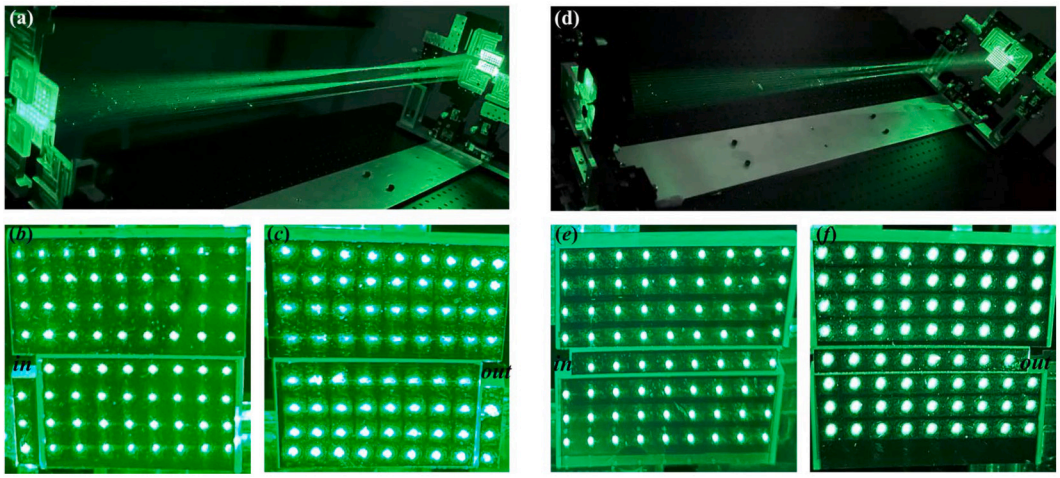

Fig. 8. Observed matrix patterns in two sets of 3-mirror SMMSs. (a)-(c)3-mirror SMMS-I. (d)-(f)3-mirror SMMS-II.

if the displacement of $C_1 \sim C_3$ on the B side is $\boldsymbol{r}$, the displacement of the odd images on the B side is $2\boldsymbol{r}$, while the positions of even images remain the same. To ensure that the emergent beam can leave through the exit hole, it is preferable to fix the outlet window at the position of the even image $mn-2$. Additionally, when the displacement of image 0 is $\boldsymbol{r}$, all the odd images' displacement is $-\boldsymbol{r}$, while all the even images' displacement is $\boldsymbol{r}$. In conclusion, under the condition that the mirrors on the same side of the SMMSs are fixed to each other, the image position errors do not accumulate, and the stability of the final image is high.

4.1.2. Matrix deviation and beam quality analysis

If the system has a shorter base length, the deviation of the light from the optical axis is greater, thus the distortion of the matrix patterns is more serious. We also used ray tracing simulation software to model the parameters of the SMMSs used in our experiments.

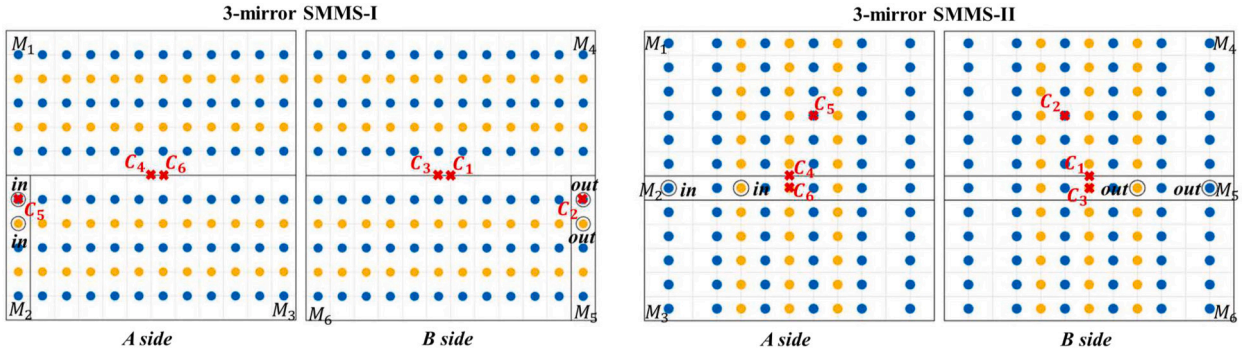

Fig. 9. Examples of dual-laser channel SMMSs. Each color represents the images of one particular laser channel. The red crosses are the curvature centers.

The simulation reveals that the circular light spots exhibited minimal distortion and were uniformly distributed as a perfect matrix. In the design of SMMS, it is necessary to optimize the distance of light spot from the axis and the angle between light and optical axis to ensure that the paraxial approximation conditions are met. This constraint helps ensure the integrity of the light spot matrix without distortion. Otherwise, the effect of aberration on the measurement effect needs to be considered, which can lead to significant distortion in the shape of the matrix light spots and may even cause the light to exit through gaps or the edges of the mirrors. In order to satisfy the condition of paraxial approximation, we set d and R to 1000 mm and limited the largest total length of one side of the mirrors to 50 mm.

Two sets of SMMSs have been successfully built in the laboratory. Fig. 8 presents the matrix patterns with 8 rows and 9 columns on both sides of the two 3-mirror SMMSs. Fig. 8(a) and (d) show the setups of SMMS-I and SMMS-II, respectively. The matrix patterns on the inlet and outlet sides of SMMS-I are shown in Fig. 8(b) and (c), respectively, while those of SMMS-II are shown in Fig. 8(e) and (f). It is clear that the beam spots of a semiconductor laser have no noteworthy distortion. The images remain the same on each side of the two systems, and the images on the A side are smaller than those on the B side. This observation is in great agreement with the theory that only two beam shapes will appear alternately and remain constant after any number of reflections in a perfectly confocal cavity [37]. Consequently, SMMSs have a great tolerance for the dimension of the images and the exact waist of the laser beam. In contrast to the Herriott cell, the 3-mirror SMMSs based on the confocal properties have a longer optical path length and lower field aberration. This makes them suitable for working in a cylindrical unit of a high-resolution infrared laser spectrometer [25].

4.1.3. Multi-laser channel analysis

Multispecies trace gas sensing is becoming increasingly important in a diverse range of applications. The newly designed SMMSs have the attractive character of special symmetric configurations, which offers convenience to design multiple independent laser channels of different optical path lengths. It can measure the concentration of various gases simultaneously. Fig. 9 shows the examples of dual-laser channel SMMS-I and II.

On mirror M_2 and M_5, there are two pairs of inlet windows and outlet windows used to form two laser channels, which do not interfere with each other and have different optical path lengths. Because the inlet and outlet windows are located on different sides of the system, it is easy to assemble and adjust the laser and receiver devices. The formation orders of the matrix patterns of each channel conform to the law described above. The multi-channel gas cell helps to realize the multi-range detection of one gas or the simultaneous detection of several gases [12,13,38]. By introducing two laser beams of different wavelengths into the dual channels, our system can simultaneously measure gases with distinct absorption wavelengths. Each channel, having different optical path lengths, is tailored to detect gases within different concentration ranges. This makes our system suitable for simultaneously measuring gases with varying detection limits. The pathlength of the blue images in Fig. 9 is longer, which is suitable for detecting gases with lower concentrations. It should be noted that more laser channels can be configured in the SMMSs if needed.

4.2. Experimental verification and analysis of 4-mirror SMMS

A 4-mirror SMMS is built and the reflection order of the matrix pattern is demonstrated by the experimental results. The matrix pattern with 4 rows and 8 columns observed in the experiment is shown in Fig. 10, which is consistent with the calculation of the theoretical matrix pattern and forming order shown in Fig. 7 (a).

The 3-mirror SMMSs and the 4-mirror SMMS all have charming symmetrical structures and separate inlet/outlet windows at two sides of the systems. This advantage makes SMMSs promising MPCs for multi species detection by establishing independent multi-laser channels with different optical path lengths. With the same base length and matrix size, a 4-mirror SMMS has a longer optical path length owing to its overlapping matrix patterns, while 3-mirror SMMSs are easier to adjust because of the simpler laws of reflection. In accordance with their characteristics, an appropriate SMMS can be chosen easily to satisfy the practical measurement. This study demonstrates that the proposed design methodology can be further extended to more complex SMMSs design and optimization.

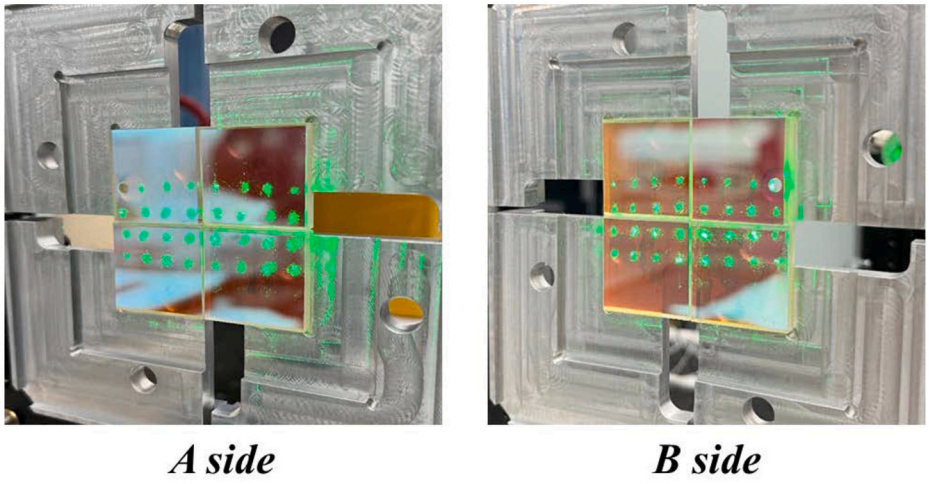

Fig. 10. Observed matrix patterns after 105 passes of semiconductor laser radiation in the 4-mirror SMMS.

5. Conclusion

In conclusion, we propose a new type of multipass cell named symmetric optical multipass matrix system (SMMS), in which the same matrix patterns with various sizes can be formed on both sides. In addition to inheriting all the advantages of chernin-type MMS, the newly designed SMMSs have the attractive character of special symmetric configurations. The optical path length of SMMSs is adjustable in a wide range, from a few meters to several hundred meters easily, merely depending on the size of the matrix. The special virtues of SMMSs offer great convenience to design multi-laser channels for simultaneous multi species trace gas sensing. By modeling the SMMS design problem as a variant of the classical traveling salesman problem, two original 3-mirror SMMSs are designed, analyzed and built.

The proposed method is further extended to design a 4-mirror symmetric optical MMS. The experimental observations are in good agreement with the theoretical calculations, which verifies the effectiveness and robustness of the design methodology. Altogether, the newly proposed SMMSs have a promising application prospect in trace gas measurement. And the strategy we put forward promise to promote the design and development of the multipass matrix systems.

Funding

Beijing Normal University (10100-312232102).

CRediT authorship contribution statement

Xiangjun Xiao: Writing – original draft, Methodology. **Miyun Shi:** Software, Investigation. **Jingjing Qiu:** Visualization, Validation. **Xue Ou:** Project administration, Data curation. **Peng Liu:** Validation, Investigation. **Xin Zhou:** Writing – review & editing, Methodology, Conceptualization.

Declaration of competing interest

The authors declare that they have no known competing financial interests or personal relationships that could have appeared to influence the work reported in this paper.

Data availability

Data underlying the results presented in this paper are not publicly available at this time but may be obtained from the authors upon reasonable request.

Acknowledgements

This work was supported by the Scientific Research Foundation of the High Level Scholars of Beijing Normal University (10100-312232102).

Appendix A. Supplementary material

Supplementary material related to this article can be found online at https://doi.org/10.1016/j.heliyon.2024.e34682.

References

[1] Yingchun Cao, Nancy P. Sanchez, Wenzhe Jiang, Robert J. Griffin, Frank K. Tittel, Simultaneous atmospheric nitrous oxide, methane and water vapor detection with a single continuous wave quantum cascade laser, Opt. Express 23 (3) (2015) 2121–2132.

[2] Y. Yu, N.P. Sanchez, R.J. Griffin, F.K. Tittel, CW EC-QCL-based sensor for simultaneous detection of H_2O, HDO, N_2O and CH_4 using multi-pass absorption spectroscopy, Opt. Express 24 (10) (2016) 10391–10401.

[3] Z. Du, S. Zhang, J. Li, N. Gao, K. Tong, Mid-infrared tunable laser-based broadband fingerprint absorption spectroscopy for trace gas sensing: a review, Appl. Sci. 9 (2) (2019).

[4] Zhenzhen Wang, Wangzheng Zhou, Takahiro Kamimoto, Yoshihiro Deguchi, Junjie Yan, Shunchun Yao, Krunal Girase, Min-Gyu Jeon, Yoshiyuki Kidoguchi, Yuzuru Nada, Two-dimensional temperature measurement in a high-temperature and high-pressure combustor using computed tomography tunable diode laser absorption spectroscopy (CT-TDLAS) with a wide-scanning laser at 1335–1375 nm, Appl. Spectrosc. 74 (2) (2019) 210–222.

[5] L. Sun, M. Zou, Z. Yang, X. Ming, Acetylene sensing system based on wavelength modulation spectroscopy using a triple-row circular multi-pass cell, Opt. Express 28 (8) (2020).

[6] T. Wei, H. Wu, L. Dong, R. Cui, S. Jia, Palm-sized methane TDLAS sensor based on a mini-multi-pass cell and a quartz tuning fork as thermal detector, Opt. Express 29 (8) (2021).

[7] J. Xia, C. Feng, F. Zhu, S. Ye, H.A. Schuessler, A sensitive methane sensor of a ppt detection level using a mid-infrared interband cascade laser and a long-path multipass cell, Sens. Actuators B, Chem. 334 (30) (2021) 129641.

[8] B.C. Wang, H.X. Li, Q. Zhang, Decomposition-based multiobjective optimization for constrained evolutionary optimization, IEEE Trans. Syst. Man Cybern. Syst. 51 (1) (2018) 574–587.

[9] Ruyue Cui, Lei Dong, Hongpeng Wu, Shangzhi Li, Xukun Yin, Lei Zhang, Weiguang Ma, Wangbao Yin, Frank K. Tittel, Calculation model of dense spot pattern multi-pass cells based on a spherical mirror aberration, Opt. Lett. 44 (5) (Mar 2019) 1108–1111.

[10] Jiahao Liu, Yuze Chen, Lin Xu, Rong Kong, Peng Liu, Xin Zhou, Generalized optical design and optimization of multipass cells with independent circle patterns based on the Monte Carlo and Nelder-Mead simplex algorithms, Opt. Express 29 (13) (Jun 2021) 20250–20261.

[11] R. Claude, Simple, stable, and compact multiple-reflection optical cell for very long optical paths, Appl. Opt. (2007).

[12] Ming Dong, Chuantao Zheng, Dan Yao, Guoqiang Zhong, Frank K. Tittel, Double-range near-infrared acetylene detection using a dual spot-ring Herriott cell (DSR-HC), Opt. Express 26 (9) (2018) 12081.

[13] Christopher G. Tarsitano, Christopher R. Webster, Multilaser Herriott cell for planetary tunable laser spectrometers, Appl. Opt. 46 (28) (2007) 6923.

[14] D. Herriott, H. Kogelnik, R. Kompfner, Off-axis paths in spherical mirror interferometers, Appl. Opt. 3 (4) (1964) 523–526.

[15] John U. White, Long optical paths of large aperture, J. Opt. Soc. Am. (1917–1983) 32 (5) (1942) 285.

[16] Shiling Feng, Xuanbing Qiu, Guqing Guo, Enhua Zhang, Qiusheng He, Xiaohu He, Weiguang Ma, Christa Fittschen, Chuanliang Li, Palm-sized laser spectrometer with high robustness and sensitivity for trace gas detection using a novel double-layer toroidal cell, Anal. Chem. 93 (10) (2021) 4552–4558.

[17] Hong Chang, Shiling Feng, Xuanbing Qiu, Huiyan Meng, Guqing Guo, Xiaohu He, Qiusheng He, Xiaohua Yang, Weiguang Ma, Ruifeng Kan, Christa Fittschen, Chuanliang Li, Implementation of the toroidal absorption cell with multi-layer patterns by a single ring surface, Opt. Lett. 45 (21) (Nov 2020) 5897–5900.

[18] D.R. Herriott, H.J. Schulte, Folded optical delay lines, Appl. Opt. 4 (8) (1965) 883.

[19] J.B. Mcmanus, P.L. Kebabian, M.S. Zahniser, Astigmatic mirror multipass absorption cells for long-path-length spectroscopy, Appl. Opt. (1995).

[20] B. Fang, N. Yang, W. Zhao, C. Wang, W. Chen, Improved spherical mirror multipass-cell-based interband cascade laser spectrometer for detecting ambient formaldehyde at parts per trillion by volume levels, Appl. Opt. 58 (32) (2019) 8743.

[21] Biao Cao, Huajun Yang, Ping Jiang, Weinan Caiyang, Miaofang Zhou, Shengqian Mao, Yan Qin, Modified ray transfer matrix method for accurate non-sequential ray tracing between arbitrary reflective mirrors, Opt. Express 28 (12) (Jun 2020) 17732–17740.

[22] R. Kong, T. Sun, P. Liu, X. Zhou, Optical design and analysis of a two-spherical-mirror-based multipass cell, Appl. Opt. 59 (6) (2020).

[23] Ruyue Cui, Lei Dong, Hongpeng Wu, Weiguang Ma, Liantuan Xiao, Suotang Jia, Weidong Chen, Frank K. Tittel, Three-dimensional printed miniature fiber-coupled multipass cells with dense spot patterns for ppb-level methane detection using a near-IR diode laser, Anal. Chem. 92 (19) (2020) 13034–13041.

[24] Lorenzo Grassi, Rodolfo Guzzi, Theoretical and practical consideration of the construction of a zero-geometric-loss multiple-pass cell based on the use of monolithic multiple-face retroreflectors, Appl. Opt. 40 (33) (Nov 2001) 6062–6071.

[25] S.M. Chernin, E.G. Barskaya, Optical multipass matrix systems, Appl. Opt. 30 (1) (Jan 1991) 51–58.

[26] S.M. Chernin, S.B. Mikhailov, E.G. Barskaya, Aberrations of a multipass matrix system, Appl. Opt. 31 (6) (Feb 1992) 765–769.

[27] Semen Chernin, Promising version of the three-objective multipass matrix system, Opt. Express (2002).

[28] Semen M. Chernin, Multipass matrix systems for diode laser spectroscope, in: Proceedings of the 4th International Symposium on Monitoring of Gaseous Pollutants by Tunable Diode Lasers, Infrared Phys. Technol. 37 (1) (1996) 87–93.

[29] Y. Guo, L.Q. Sun, Z. Yang, Z. Liu, Generalized design of a zero-geometric-loss, astigmatism-free, modified four-objective multipass matrix system, Appl. Opt. 55 (6) (2016) 1435–1443.

[30] G. Yin, L. Sun, Compact optical multipass matrix system design based on slicer mirrors, Appl. Opt. 57 (5) (2018) 1174.

[31] T. Mohamed, F. Zhu, S. Chen, J. Strohaber, A.A. Kolomenskii, A.A. Bengali, H.A. Schuessler, Multipass cell based on confocal mirrors for sensitive broadband laser spectroscopy in the near infrared, Appl. Opt. 52 (29) (2013) 7145–7151.

[32] H.J. Bernstein, Gerhard Herzberg, Rotation-vibration spectra of diatomic and simple polyatomic molecules with long absorbing paths. I. The spectrum of fluoroform (CHF_3) from 2.4μ to 0.7μ, J. Chem. Phys. 16 (1948) 30–39.

[33] David C. Tobin, L. Larrabee Strow, Walter J. Lafferty, W. Bruce Olson, Experimental investigation of the self- and N_2-broadened continuum within the $\nu 2$ band of water vapor, Appl. Opt. 35 (24) (Aug 1996) 4724–4734.

[34] Richard E. Shetter, James A. Davidson, Christopher A. Cantrell, Jack G. Calvert, Temperature variable long path cell for absorption measurements, Rev. Sci. Instrum. 58 (1987) 1427–1428.

[35] M. Semen, Chernin, Development of optical multipass matrix systems, J. Mod. Opt. 48 (4) (2001) 619–632.

[36] Y. Wang, Z. Li, X. Liu, F. Fang, X. Zhang, Freeform-objective Chernin multipass cell: application of a freeform surface on assembly simplification, Appl. Opt. 56 (30) (2017) 8541–8546.

[37] G. Manuel, E. Lukas, T. Béla, Compact, circular, and optically stable multipass cell for mobile laser absorption spectroscopy, Opt. Lett. 43 (11) (2018) 2434.

[38] Gui-sheng Jiang, Yuting Wang, Qiang Liu, Hang Chen, Shi-qi Wang, Yu Zhang, Zhao-xiang Wang, Hui Zhang, Shenlong Zha, Ya Wang, Hongqiang Ma, Methane gas sensor based on a novel dual-path multipass cell, Microw. Opt. Technol. Lett. 66 (2023).